



## FINITE-ELEMENT MODELING AND OPTIMIZATION OF THE DEEP ROLLING PROCESS WITH A TOROIDAL ROLLER IN ALUMINUM ALLOY 2024-T3

Galya Duncheva\*, Tihomir Atanasov

Technical University of Gabrovo, Gabrovo, Bulgaria

### ARTICLE INFO

#### Article history:

Received 12 August 2019

Accepted 5 September 2019

#### Keywords:

deep rolling; toroidal roller; 2024-T3 aluminum alloy; planned numerical experiment; axial residual stress distribution; dispersion analysis; regression analysis; process optimization

### ABSTRACT

*In this article the deep rolling with toroidal roller of cylindrical specimens made of 2024-T3 high-strength aluminum alloy was studied and optimized in terms of the useful residual axial stress distribution. For this purpose, a planned numerical experiment was conducted, based on developed 3D finite element model of the process being studied. The surface layer constitutive model was defined in accordance with the flow stress concept. The governing factors are the radius of roller curvature, the feed rate, and the burnishing force magnitude. The objective functions are the residual axial stresses in the middle of the surface being treated and the average value of the residual axial stresses in a depth of 0.5 mm from the surface. In order to study the objective functions, dispersion analysis (ANOVA) and regression analysis were performed. Based on the obtained regression models, the process optimization was conducted. As a result, the governing factors values providing the maximum intensive and deep zone with useful residual axial stresses were defined.*

© 2020 Journal of the Technical University of Gabrovo. All rights reserved.

### INTRODUCTION

According to the requirements of the contemporary market, the responsible metal structural and machine elements must provide high reliability and safety during operation and minimal mass and dimensions. These requirements are leading in modern automotive, aircraft, shipbuilding and space industries, where the life time of the elements depends primarily on their fatigue and tribological behavior. In other sectors such as power generation industry and oil and gas industries, the dynamic loads are combined with significant temperature loads. In general, in the case of responsible structural components, it is necessary to predict the operational behavior in correlation with the manufacturing process.

It is known that the complex of properties of the surface layers, etc. Surface Integrity (SI), has a decisive role for the structural elements operation [1]. In fact, during the workpieces preparation stage, the improvement of SI is practically impossible. On the other hand, the various defects in the microstructure of the metals cannot be excluded. In this aspect, Surface Engineering Processes (SEP) are increasingly relevant to modify the properties of the surface layers. According to the possibility of changing the chemical composition of the material, SEP are developed in three main directions:

I. Modification of the surface layers based on diffusion of new chemical elements into them by means of so-called Thermochemical Diffusion Processes (TDP); The original chemical composition has a main role in the modified layer. In this case chemical-thermal treatments such as carburizing, nitriding, cyanation, etc are used;

II. Modification by adding a new material to the surface in the form of coatings; This approach aims to create a barrier between the coating layer and the environment;

III. Modification of the surface layers without alteration in the material chemical composition; In this direction, SEP are based on two approaches: Surface Heat Treatment (SHT); Mechanical Surface Treatment (MST).

SHT processes and TDP result in phase transformations in the material that are the physical basis for the modification of the surface layers. These processes have established themselves as conventional techniques used primarily to increasing the hardness and wear resistance of the surface layers. On the one hand, this kind of processing is costly time-consuming and non-ecological and, on the other hand, it is not efficient enough to improve the operation in general and, in particular, the fatigue behavior of the components. Modern processes providing a greater value for cost/quality ratio are MST processes for surface plastic deformation.

In terms of kinematics, the processes for surface plastic deformation are similar to the turning, as the tool comprises a rigid and smooth deforming sphere or roller. The tool is pressed against the rough surface being treated until to complete plasticizing of the surface layers. Significant local plastic deformation of the micrograph peaks changes the surface topography reducing the micrographs ("burnishing effect"). At the same time, due to the high density of the dislocations, the superficial and subsurface layers are subjected to cold working and the microstructure is modified.

\* Corresponding author. E-mail: duncheva@tugab.bg

Since these processes are conducted at the ambient temperature, the force contact interaction between the deforming elements and the surface being treated is dominated in comparison with the temperature effect. As a result, beneficial residual stresses are introduced in adjacent to the surface regions. Summing up, the modification of the superficial layers after plastic deformation is due to three major positive effects: significant reduction of the roughness, cold work, and induction of compressive residual stress zone. This SI combination has a proven beneficial effect on the fatigue and tribological behavior and the corrosion resistance of the components.

In practice, MST processes are effective for most ferrous and non-ferrous alloys. The methods for their implementation are dynamic and static. The static methods have a wider application since their parameters can be controlled in correlation with SI. Shot peening method which belong to the dynamic methods, has the greatest application.

The main feature of classifying the static methods is the type of contact between the deforming element and the surface being treated - sliding friction or rolling friction. According to this feature, there are two types of methods: roller burnishing and ball burnishing; slide burnishing. In the latter case, the deforming elements are predominantly synthetic polycrystalline diamonds. That's why, the diamond burnishing method is a widest application [2-7]. Comprehensive studies of the potential capabilities of this process to improve the fatigue behavior in correlation with process parameters were conducted by Maximov et al. with respect to high-strength aluminum alloys [2-5] and AISI 316Ti chromium-nickel steel [6]. On the basis of diamond burnishing, an approach for increasing the fatigue life of rail-end-bolt holes has been developed [7].

As a whole, the processes involving rolling friction contact have a greater practical application. Ecoroll, the world leader in this field, has developed a wide-ranging nomenclature for finishing tools containing deforming rollers or balls. According to Ecoroll, however, the main sign of differentiation of these processes is not the deforming element geometry (roller or ball), and the effect to be achieved in terms of performance [8]. From this point of view, Ecoroll presents two types of MST processes: roller burnishing and deep rolling. The roller burnishing process is primarily aimed to provide a minimum roughness ( $R_a \leq 0.2 \mu\text{m}$ ), as well as high form and size accuracy. Multiple and single roller tools are used for this purpose [9, 10].

The deep rolling concept is used to treat external and internal cylindrical and tapered surfaces as well as profile surfaces in dynamically loaded components. Therefore, in deep rolling, the emphasis is placed on cold work and induction of compressive residual stresses in the surface layers, and the reduction of roughness is an accompanying effect. The deep rolling process is carried out in the following variants: hydrostatic ball burnishing [11-16]; deforming ball with rigid or elastic action [17-19]; by means of a cylindrical [20-24] or a toroidal deforming roller [25-26]. In a number of scientific publications, the corresponding process is associated with the deforming element shape (ball burnishing or roller burnishing), but not with the effect on the operational characteristics [12, 13, 15, 18, 20, 21, 22, 23, 26]. For particular geometry and material of the deforming element and the workpiece, SI depends on the burnishing force magnitude  $F_b$  and the

process parameters: feed rate  $f, \text{mm/rev}$  and the workpiece rotation speed  $v, \text{m/min}$ . Obviously, by controlling the process parameters, a different combination of SI can be provided through one and the same method. In this aspect, the experimental study approach is no alternative.

The advantage of roller burnishing and deep rolling processes to improve SI and fatigue behavior compared to other finishing methods has been established with respect to broad nomenclature of constructional materials. For comparative analysis, various experimental techniques are used, most often experimental design and fatigue tests. The advantage of the roller-burnishing process compared to the electro-polishing and the shot peening in terms of surface roughness, hardness profiles and fatigue life for three types of titanium alloys is confirmed in [10]. For this purpose, hourglass shaped specimens subjected to rotating bending ( $R = -1$ ) were used.

The advantage of roller burnishing compared to shot peening in terms of fatigue strength, micro-hardness and useful residual stresses is proven for Al6061 aluminum alloy in [11]. The effect of shot peening, roller burnishing and deep rolling on the fatigue performance of a modern gamma titanium aluminides was systematically investigated in [14]. The process-induced changes in surface properties are evaluated by metallographic analysis, residual stress measurements and S-N curves of notched fatigue specimens. The S-N curves show the advantage of deep rolling up to  $2 \times 10^6$  cycles.

A comparison between the conventional deep rolling process with a hydrostatic non-assisted ball-burnishing tool, and vibration-assisted tool was done in [17]. The authors reported that significantly better average roughness of aluminum was obtained by assisting the process with vibrations. Mombeini and Atrian, (2018) conducted fatigue bending tests and fractograph analysis of brass C38500, comparing the conventional case (cylindrical specimens, machining by cutting) with specimens subjected to deep rolling with various burnishing forces [18]. The authors developed a tool containing two burnishing balls set in a special holder with the possibility of free rotation around the cylindrical surface of the specimens. It was established that deep rolling is more effective in the low cyclic fatigue than the high cyclic fatigue loading regimes for brass C38500 [18].

Majzoubi et al., (2016) have compared the bending fretting fatigue resistance of Al707 aluminum alloy with and without deep rolling for two feed rates (0.08, 0.160) and number of passes (1; 2) [19]. The resulting S-N curves show advantage of the deep rolling process when it implemented with less feed and two number of passes. Sai and Lebrun, (2003) analyzed the change in residual stresses, micro-hardness and roughness, comparing the performance of different finishing processes for duplex stainless steel: turning, grinding and deep rolling [20]. It was proven that the deep rolling process provides the best quality of the surface.

Numerous studies were focused to optimizing the process parameters to ensure minimal roughness. Using experiment design, the resulting roughness was the object of modeling for various aluminum alloys and composites: a commercial aluminum alloy [9, 23]; aluminum alloy 6061 [12]; Al-Cu alloys [13]; aluminum 2007, which material is suitable for producing machine parts, bolts and rivets [17]; high-strength aluminum alloys Al 7075-T73 and Ti-6Al-4V

used in aircraft [21]; aluminum composites based on A356 [24] and AA2124 [25], in which silicon carbide is used as the reinforcing phase. The resulting roughness after burnishing was the subject of study for a broad nomenclature of ferrous and nonferrous alloys: AISI 1060 high carbon steel [15]; 15-5PH stainless steel [15]; brass C38500 [18]; STAVAX plastic mold stainless steel [22]; mild steel [26]. In general, the effectiveness of burnishing processes on SI, including micro-hardness and beneficial compressive residual stresses, was experimentally confirmed in numerous publications [2, 3, 5, 6, 13-16, 18, 20, 21, 26].

In terms of fatigue life enhancement, the effect of creating a zone with compressive residual stresses in the superficial and subsurface layers is of decisive importance. In other words, if the burnishing effect and the cold work effect are assumed to be constant for a concrete process, the residual stress profile was proven to be of greatest importance in improving the fatigue behavior of the structural elements [2, 3, 5-7, 14-16, 18, 20, 21, 25]. Consequently, for the realistic prediction of the fatigue life, it is necessary to know in qualitative and quantitative aspects the residual stresses distribution immediately after the corresponding burnishing process. On the other hand, a main problem for researchers is the problem of assessing the relaxation of residual stress. The relaxation phenomenon may be caused by overload, temperature load or cyclic mechanical load. In general, empirical models [27, 28] and analytical models [29, 30] were proposed to estimate the residual stress relaxation due to cyclic loading.

Two main approaches are used for evaluation of the residual stresses - experimental approach and finite element method (FEM) simulations. The experimental approach was based mostly on the non-destructive X-ray diffraction method [2, 5, 6, 16, 20, 25] and the semi-destructive hole drilling method [14, 21].

Residual stress measurement by X-ray diffraction analysis is more reliable, but this technique is too expensive and time-consuming. A significant disadvantage is the low penetration depth (for example in steel, residual stresses can be measured at a depth up to 7  $\mu\text{m}$ ). In order to evaluate the residual stresses in depth, the technique for gradual removal of layers by electrolytic polishing is used. On the one hand, this technique requires a considerable amount of time and resources, and on the other hand, the removal of material layer obviously alters the strained and stressed state in the relevant element. In this aspect, numerical simulations are "effective tool" for in-depth investigation of the residual stresses created after various cold working processes since they provide a wide range of information for relatively little time without the need for material resources. To ensure reliable numerical results, it is necessary the corresponding finite element (FE) model to be maximum adequate to the research process. The main factors for this are: the realism of the geometry and the interaction between the deforming element and the workpiece; the realism of boundary conditions; the mech strategy used; the constitutive model of the material.

Significant number of publications exists based on 2D and 3D FE models of the burnishing processes [18, 31-43]. In 2D FE models, the interaction between the workpiece and the deforming ball or roller is simulated under plane strain conditions [18, 31, 35, 38, 42, 43]. As a result, the actual contact ball/cylinder on cylinder is transformed into a linear contact cylinder on a plane.

Using DEFORM-2D FEM software, Röttger, (2002) developed a 2D FE model for roller burnishing, taking into account the initial roughness of the workpiece [31]. In this model, a rigid ball is pressed down on the rough workpiece surface until the reaction force reached a predefined value that is equal to the applied burnishing force. In this way, a force control is used to simulate the burnishing process. Then, the ball was lifted up from the surface and moved horizontally by the distance of the burnishing feed. However, this force-control model would underestimate the ball penetration depth because of line contact (due to the plane strain condition).

Saï and Saï, (2005) focus on roughness obtained, combining FEM, analytical, and experimental approach [32]. The authors used 3D FE model to determine the surface layer displacements, simulating once a normal interaction between a deformable ball and a cylindrical workpiece. A comparison of the results obtained from the experiment, the analytical model from the literature (defining the parameter  $R_t$  of roughness) and those from the numerical simulations was made for two cases: elastic behavior and elasto-plastic behavior of the workpiece. In the latter case, a model of nonlinear isotropic hardening was used without a kinematic component. Thus, the accepted model of the material does not take into account the cyclic loading at the surface points of the workpiece, which is a characteristic of the burnishing processes.

Bougharriou et al., (2010) studied the surface roughness profile and the residual stresses based on 2D FE plane strain model, simulating one pass from the interaction between deformable ball and cylindrical workpiece [33]. The experimental roughness profiles after turning were taken into account in the initial mesh of the workpiece by the linear interpolation of the measured data points.

The material constitutive model in the FE models is of decisive importance for prediction of the residual stresses. In the burnishing processes the effect is applied to the surface layer at a relatively small depth. The behavior of this layer differs significantly from that of the bulk material due to the presence of large plastic deformations, a particular micro-profile of roughness, and other effects. Therefore, the conventional one-dimensional or cyclic tests are primarily representative for the bulk material behavior. To define the stress-strain dependence in the plastics field for the surface layers, the flow stress concept is used [34, 35, 2, 5-7]:

$$\sigma = \sigma_Y \left( 1 + \frac{E}{\sigma_Y} \varepsilon_p \right)^n, \quad (1)$$

where:  $\sigma$  is the "flow stress";  $\sigma_Y$  is the yield limit;  $E$  is the Young's modulus;  $\varepsilon_p$  is the plastic strain;  $n$  defines the strain hardening for one-dimensional stressed state.

Yen et al., (2005) developed 2D and 3D FEM models for hard roller burnishing of hardened AISI52100 steel using DEFORM-2D and DEFORM-3D software [34]. The authors take into account the calculated surface roughness profile (kinematic roughness). The burnishing process was simulated using displacement control. The behavior of the surface layer was defined using the flow stress concept [34]. The surface curvature effect of a cylindrical workpiece and the effect of helical cutting path angle were neglected in 3D model. Ten cycles were simulated in order to take into account the full deformation history of a single surface asperity during burnishing. It was found that the 2D

model provides a more realistic assessment of residual stresses.

Sartkulvanich et al., (2007) improved 2D and 3D KE models of hard roller burnishing of hardened AISI 52100 steel, focusing on the flow stress [35]. In order to realistically define flow stress for roller burnishing simulations, a procedure including an instrumented indentation test and inverse KE analysis was performed.

In order to account the three-dimensional stressed state, a 3D FE model of the roller burnishing process of 11SMn30 alloyed steel was proposed in [36]. The strategy for the computational time optimizing involved modeling a representative portion of the cylindrical workpiece and inversion of the actual kinetics of the roller burnishing process (analogous to that of turning). The boundary conditions were transmitted to the roller via connectors in Abaqus FEM software. The corresponding stress-strain reference curve is determined using Rastegaev-type compression sample. However, this test is representative for the behavior of the bulk material, not for the surface layer. The proposed model was validated by comparing the numerical results for axial and hoop residual stresses with experimentally obtained by X-ray diffraction analysis.

The described strategy was used by Trauth et al., (2013) for developing a 3D KE model of the deep rolling process of three types of high-strength alloys: IN718 (ASTM: B637), 42CrMo4 (ASTM: A322-44040), GGG60 (ASTM: A536 -80-55-06) [37]. It was done a transfer of the rotational movement of the workpiece to the spherical tool. The explicit solver suitable for dynamic problems was chosen using Simulia Abaqus 6.12. A material model of non-linear isotropic and kinematic hardening was used.

Sayahi et al., (2013) investigated burnishing of Ti-6Al-7Nb alloy based on 2D and 3D FE models using tool displacement control [38]. In both FE models the surface roughness profile and the ball burnishing speed were neglected. The deforming ball was accepted as a rigid body. In 3D model the workpiece was modelled by a portion of a cylindrical part and ABAQUS/explicit was used. The results were obtained using the isotropic hardening material model. Thus, in FEM simulations the effects of ball burnishing speed were neglected, which in itself the dynamic analysis.

Using ABAQUS/Explicit 3D FE study was conducted of a flat specimen made of Ti-6Al-4V alloy, which is processed by low plasticity burnishing [39]. Taking into account the temperature effect and the effect of strain rate, the authors adopted the Johnson-Cook material constitutive model. The developed FE model was used to investigate the effect of main parameters including ball diameter, burnishing force, burnishing feed, and number of passes on the resultant profile of the residual stresses and plastic strain. Zhuang and Wicks, (2004) were proposed non-linear moving contact 3D FE model to simulate the multipass low plasticity burnishing on a flat specimen made of IN 718 high-strength alloy [40]. The constitutive model used in this study is a non-linear isotropic/kinematic hardening model. The material parameters were calibrated from the cyclic stress/strain response obtained from experimental measurements on the material.

The final roughness and residual stresses distribution in the surface layers after ball burnishing process was studied in [41]. The 3D random roughness model in the surface of cylindrical bars is generated by using a computational routine based on ANSYS Parametric Design Language. The

computational routine generates a 3D rough surface by extrusion the area generated. A bilinear isotropic material with the mechanical properties of AISI 1045 steel was used. In this FE model, only the deforming ball penetration was simulated, i.e. the cyclical loading caused by overlapping of the contact areas due to the feed was not taken into account.

A 2D FE study of the roughness evolution after burnishing of AISI D3 tool steel was conducted by John et al., (2016) [42]. For that purpose, the measured roughness profile after turning was approximated as sinusoidal using DEFORM-2D software. The FE results for final roughness were compared with experimental outcomes.

The influence of the feed on the overlapping effect of the contact areas in the slide burnishing of titanium alloy was investigated by He et al., (2018) [43]. Based on 2D FE study it was found that the overlapping effect was more pronounced with feed rate decreasing.

The review of scientific publications related to FEM studies of various burnishing processes shows that deforming impacts with spherical or cylindrical deforming tools are examined in a broad nomenclature of construction materials. In the literature there is a lack of FE studies of deep rolling process when the deforming element is a profiled toroidal roller.

The purpose of this article is to optimize the deep rolling process with toroidal roller in cylindrical specimens made of 2024-T3 high-strength aluminum alloy in terms of the distribution of useful residual axial normal stresses. 2024-T3 aluminum alloy is widely used in dynamically loaded components in machine building and aerospace since it has high strength to weight ratio, high corrosion resistance and good workability. In order to achieve the main goal, the following main tasks have been solved:

- 1). Conduction of planned numerical experiment based on the 3D FE model of the research process;
- 2). Modeling of the residual axial stresses in the surface and subsurface layers;
- 3). Optimization of the process in terms of the beneficial residual axial stresses distribution.

## 2. PLANNED NUMERICAL EXPERIMENT

### 2.1. Details of the planned numerical experiment

Numerous experimental and numerical studies of different burnishing processes show that burnishing speed has a limited impact on SI. This is also confirmed for the slide burnishing process of 2024-T3 aluminum alloy [2, 3]. For this reason, the rotation speed is excluded from the governing factors in the planned numerical experiment.

On the other hand, the radius  $r$  of curvature of the outer toroidal surface of the roller is much greater in comparison with the practically rational values of the feed rate  $f$ . Consequently, in the generatrix direction of the cylindrical surface of the workpiece, an overlapping effect of the contact zones between the deforming element and the surface being treated is obtained. As a result, even after one pass, the points of the surface layers are subjected to cyclic hardening ("loading-unloading" is one cycle).

Under equal other conditions, the cyclic hardening depends on the feed rate  $f$ . Consequently, the feed rate has a decisive impact on the distribution of residual stresses. On this basis, the following governing factors are chosen: radius of curvature of the toroidal surface of the roller  $r, mm$ ; feed rate  $f, mm/rev$ ; burnishing force

magnitude  $F_b, N$ . The governing factors and their levels in natural and coded coordinates are shown in Table 1.

**Table 1** Governing factors and their levels

Governing factors	Levels	
	Natural	Coded
Radius of curvature of the toroidal surface of the roller, $r, mm$ ( $x_1$ )	2	-1
	4	0
	6	+1
Feed rate, $f, mm/rev$ ( $x_2$ )	0.04	-1
	0.08	0
	0.12	+1
Burnishing force magnitude, $F_b, N$ ( $x_3$ )	600	-1
	900	0
	1200	+1

The residual axial stress  $\sigma_z^{res}$  distribution was studied in a generatrix direction from the cylindrical surface obtained after simulation of 14 cycles (Fig. 1). Each cycle includes the following roller displacements sequence: radial displacement for penetration into the workpiece until the corresponding burnishing force is reached; reverse radial displacement providing a small clearance between the roller and the workpiece; axial displacement distance equal to the feed rate. In accordance with the experimental plan from each simulation, the residual axial stresses in the middle of the treated portion of the workpiece were determined. In order to ensure correct FE results, this point is one and the same for all numerical simulations - it is denoted as  $A_{mid}$  in Fig. 1. For this purpose, the initial roller position  $A_{init}$  and the final roller position  $A_{fin}$  were changed depending on the feed rate  $f$  in the simulations (Fig. 1).

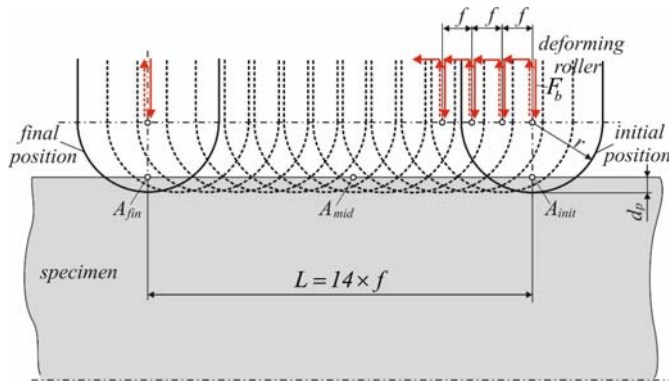


**Fig. 1.** Scheme for simulating the roller-workpiece interaction

An optimal compositional plan (Table 2) was chosen to carry out the planned numerical experiment. For each experiment point, the information for the residual axial stresses was systematized from the FE results as follows:

- $\sigma_{z,sur}^{res}$  is the residual axial stress on the surface reported for point  $A_{mid}$ ;
- $\bar{\sigma}_z^{res}$  is the calculated mean value of the residual axial stresses in depth of  $0.5 mm$  from the surface layer. For this purpose, the residual stresses corresponding to the first five nodes with the starting node coinciding with the  $A_{mid}$  were determined.

The values for  $\sigma_{z,sur}^{res}$  and  $\bar{\sigma}_z^{res}$  form the objective functions in the planned numerical experiment (Table 2).

**Table 2** Numerical experiment design

$N^{\circ}$	$x_1$	$x_2$	$x_3$	$\sigma_{z,sur}^{res}, MPa$	$\bar{\sigma}_z^{res}, MPa$
1	-1	-1	-1	-236.11	-161.52
2	+1	-1	-1	-170.21	-127.91
3	-1	+1	-1	-284.70	-155.71
4	+1	+1	-1	-233.89	-136.91
5	-1	-1	+1	-211.27	-228.35
6	+1	-1	+1	-125.94	-202.12
7	-1	+1	+1	-325.83	-240.41
8	+1	+1	+1	-259.04	-212.56
9	-1	0	0	-302.02	-215.23
10	+1	0	0	-212.80	-182.26
11	0	-1	0	-181.37	-185.11
12	0	+1	0	-275.97	-187.52
13	0	0	-1	-260.77	-154.40
14	0	0	+1	-230.67	-222.36

## 2.2. FE modeling

In fact, in burnishing process with toroidal roller the stressed state and strained state are three-dimensional. In order to obtain a realistic residual stresses information, a generalized 3D FE model of the studied process was developed using Abaqus/CAE2018 (Fig. 2). The outer diameter of the toroidal roller ( $D = 26 mm$ ) was adopted on the basis of preliminary experiments, design restrictions related to special burnishing device, and the results obtained from a numerical study of the equivalent plastic strain in the 2024-T3 aluminum alloy [44]. The deforming roller was adopted as rigid body in the developed FE model (Fig. 2).

The residual axial stresses  $\sigma_z^{res}$  in cylindrical workpiece with a diameter of  $20 mm$  were examined. The workpiece was symmetrically loaded with respect to a plane containing its axis. Therefore, a half of the workpiece was modeled. For all workpiece surfaces, except the outer cylindrical surface, an elastic foundation was set with a stiffness equal to the Young's modulus of the alloy being studied. Thus, the interaction with the neighboring, elastically deformed layers of the material was simulated (Fig. 2).

A relatively small length of the workpiece  $5 mm$  was modeled. The reasons for this are the following. The studied burnishing process is characterized by a very large strain gradient in the radial direction and the contact area dimensions are much smaller than the workpiece sizes. Therefore, it can be assumed that the deforming effect is independent by the outer boundaries of the workpiece. During the deep rolling process, the entire cylindrical surface of the workpiece is crawled by the roller. This contact is implemented in an identical way at any time in the process. Therefore, the entire process can be simulated through modeling just a small part of the workpiece.

The workpiece mesh was one and the same in all numerical simulations. The FE mesh was refined in the contact area (Fig. 2). A total of 7245 nodes and 6240 FEs were used to model the workpiece, of which 6220 linear hexahedral FEs of type C3D8R and 20 linear vedge FEs of type C3D6. The radius of curvature of the roller  $r$  and the burnishing force magnitude  $F_b$  were changed in accordance with the experimental plan.

The burnishing process is simulated using displacement control of the roller. The displacements in the radial (Z-axis) and axial direction (Y-axis) were defined by pseudo-time tabulated functions related to the roller Reference

Point (RP) (Fig. 2). Preliminary FE simulations were performed to define the dependence between the burnishing force  $F_b, N$  and the depth of penetration  $d_p, mm$ . The dependence  $F_b = F_b(d_p)$  for the three values of the radius in a tabulated form is shown in Table. 3. The material is elasto-plastic and strain independent. Poisson coefficient  $\nu = 0.33$  was set.

**Table 3**  $F_b = F_b(d_p, r)$  dependence in a tabulated form

$F_b, N$	$r = 2 mm$	$r = 4 mm$	$r = 6 mm$
	$d_p, mm$	$d_p, mm$	$d_p, mm$
600	0.041	0.034	0.03
900	0.058	0.045	0.04
1200	0.071	0.0575	0.05

The surface layer constitutive model of the studied aluminum alloy is defined in accordance with the flow stress concept [45]. The flow stress model of the workpiece surface and subsurface layers was obtained in the form of Eq. (1). The constants in the earlier equation were obtained by means of instrumented indentation test and subsequent inverse FEM analysis. The instrumented indentation test physically corresponds to the Brinell hardness test. A small diameter spherical nozzle is clamped into an asymmetric specimen under axial force  $P$  so that the loading pattern is asymmetrical. The specimen is a cylindrical body made of aluminum alloy 2024-T3 (Fig. 3a). Successively an axial force of 20, 40, 60, 80, 100, 120 N is applied and the diameter of the spherical nozzle is 2.5 mm. As a result, the experimental dependence  $P = P(d^{res})$  is obtained, where  $d^{res}$  is the spherical imprint depth. This dependence is used as a criterion in the subsequent inverse FE analysis to define the unknown parameters  $\sigma_Y$  and  $n$  in the equation (1). For this purpose an asymmetrical 2D FE model is used (Fig. 3b).

Based on the sequential experimental indentation test and inverse FEM analysis, the material parameters in Eq. (1) are determined:

$$\sigma = 310 \left( 1 + \frac{72000}{310} \varepsilon_p \right)^{0.09} \quad (2)$$

Eq. (2) consists  $\sigma - \varepsilon$  data obtained from the instrumented indentation test and next inverse FEM analysis. The stress/strain measure in Abaqus/CAE is „true stress - logarithmic strain”. Since Eq. (2) is obtained through experiment and inverse FEM analysis, in fact  $\sigma - \varepsilon$  data are “true stress-logarithmic strain”. On the other hand, the

cyclic hardening in the vicinity of a point of the surface layer causes a deformation anisotropy. It is characterized by an irregular expansion or contraction with the movement of the yield surface in the stress space. This effect was taken into account by defining a model of non-linear kinematic hardening [46]:

$$\dot{\alpha}_{ij} = \frac{C}{\sigma^0} \sigma_{ij}^a \dot{\varepsilon}_p - \gamma \alpha_{ij} \dot{\varepsilon}_p, \quad (3)$$

where:  $\sigma^0$  is an equivalent stress defining the yield surface size, with initial size  $\sigma|_0 = \sigma_Y$  ( $\sigma|_0$  is an equivalent stress defining the yield surface size for zero equivalent plastic deformation  $\bar{\varepsilon}_p$ );  $\sigma_{ij}^a = \sigma_{ij} - \alpha_{ij}$ ,  $\sigma_{ij}$  is a stress tensor;  $\alpha_{ij}$  is a micro-stress tensor;  $C$  is an initial modulus of kinematic hardening;  $\gamma$  is a coefficient determining the rate decreasing of the kinematic hardening modulus with plastic strain increasing. The point set  $\sigma - \varepsilon$  were entered in Abaqus and “half cycle” option was used.

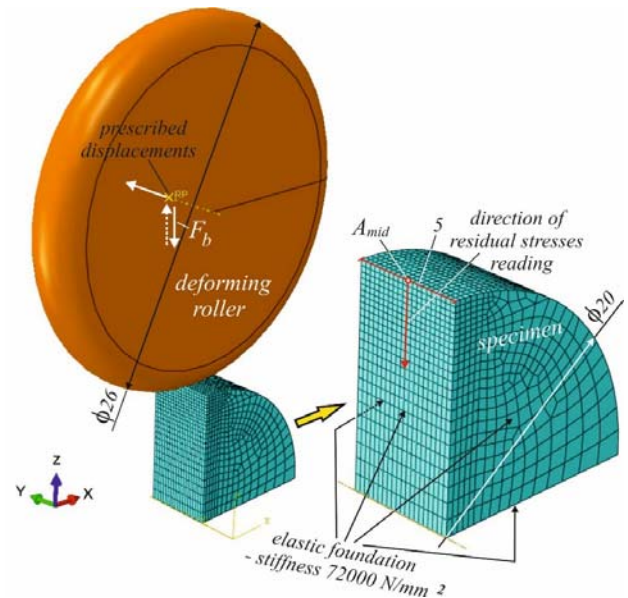
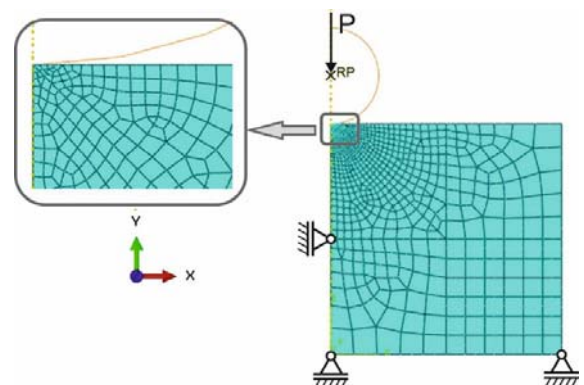


Fig. 2. Generalized 3D FE model



a). photo;



b). FE model used for inverse analysis

Fig. 3. Indentation test

### 2.3. FE results and comments

The residual axial stresses distribution in radial direction in the treated zone middle was reported. Graphs visualizing the distribution of  $\sigma_z^{res}$  in depth for the three values of  $r$  starting from the surface (p.  $A_{mid}$ ) are shown in Fig. 4a, b, c. Based on Fig. 4, the following comments can be made:

- For constant radius of curvature of the toroidal roller, the change of feed rate  $f$  and burnishing force  $F_b$  in the examined ranges significantly alters the residual axial stress  $\sigma_z^{res}$  profile;

- The radius of roller curvature  $r$  and the feed rate  $f$  strongly affect on the residual surface axial stresses  $\sigma_{z,sur}^{res}$ .

The change of  $f$  in the studied range causes a scattering of  $\sigma_{z,sur}^{res}$  about 230 MPa for  $r = 2\text{ mm}$  and about 270 MPa for  $r = 6\text{ mm}$ . The feed rate decreasing reduces  $\sigma_{z,sur}^{res}$  in absolute value, as this reduction is the greatest when the process is performed with minimum feed and maximum burnishing force. A maximum value of compressive residual stresses on the surface is obtained when the process is performed with a minimum radius, maximum feed and maximum burnishing force;

- The combination of minimum feed rate and maximum burnishing force changes the profile of the residual stress zone, as the largest absolute value  $\sigma_{z,sur}^{res}$  is obtained at a depth of  $\approx 0.5\text{ mm}$  from the surface.

### 2.4. FE results validation

In order to validate the FE model and the material constitutive model used a comparison between the FE results for residual axial stresses distribution and experimentally measured one was made. Residual axial stresses were measured by means of X-ray diffraction method. X-ray diffraction is an expensive and time consuming method. That's why one cylindrical specimen made of 2024-T3 aluminum alloy with diameter of 20 mm and length of 30 mm was burnished after turning with the following parameters:  $r = 4\text{ mm}$ ,  $f = 0,08\text{ mm/rev}$ ,  $F_b = 600\text{ N}$ . These burnishing parameters correspond to experimental point № 13 in the numerical experiment design (Table 2). The deep rolling process was implemented by a specially designed device comprising a toroidal deforming roller with an outside diameter of 26 mm as in the FE model. (Fig. 5).

In order to analyze the stress gradients beneath the specimen surface, the layers of material were gradually removed by electrolytic polishing. Residual axial stresses were measured in the Technical university in Prague. Diffraction measurements were carried out on a vertical  $\theta/\theta$  X'Pert PRO MPD diffractometer with a pin-hole collimator  $0.5 \times 1.0\text{ mm}^2$  in the primary beam. Positioning of the measured specimen to the required locations was done by combining versatile positioning system with six degrees of freedom and laser triangulation for precise surface position determination with accuracy of approximately  $5\text{ }\mu\text{m}$ . Since the effective penetration depth of used  $CrK\alpha$  radiation into the investigated alloy is only approximately  $8\text{ }\mu\text{m}$ , a biaxial state of stress was assumed, and the „ $\sin^2\psi$ “ method with least squares fitting procedure was used to evaluate

residual stresses. The measured diffraction profile of Al {311} planes has for the used filtered  $CrK\alpha$  radiation; its maximum at  $2\theta \approx 139.5^\circ$ . Diffraction profiles were fitted by Pearson VII function, and lattice deformations were calculated. In the generalised Hooke's law, Winholtz&Cohen method and X-ray elastic constants  $s_1 = 4.89 \times 10^{-6}\text{ MPa}^{-1}$  and  $1/2s_2 = 19.05 \times 10^{-6}\text{ MPa}^{-1}$  were utilised. Moreover, the diffraction profile corresponding to Al {311} planes parallel with the surface was characterized by FWHM (Full Width at Half Maximum) profile parameter which could be interpreted as „degree of plastic deformation“, because the diffraction profile broadening relates to such materials characteristics as grain size, microscopic residual stresses or dislocation density whose evolution is closely connected with plastic deformation.

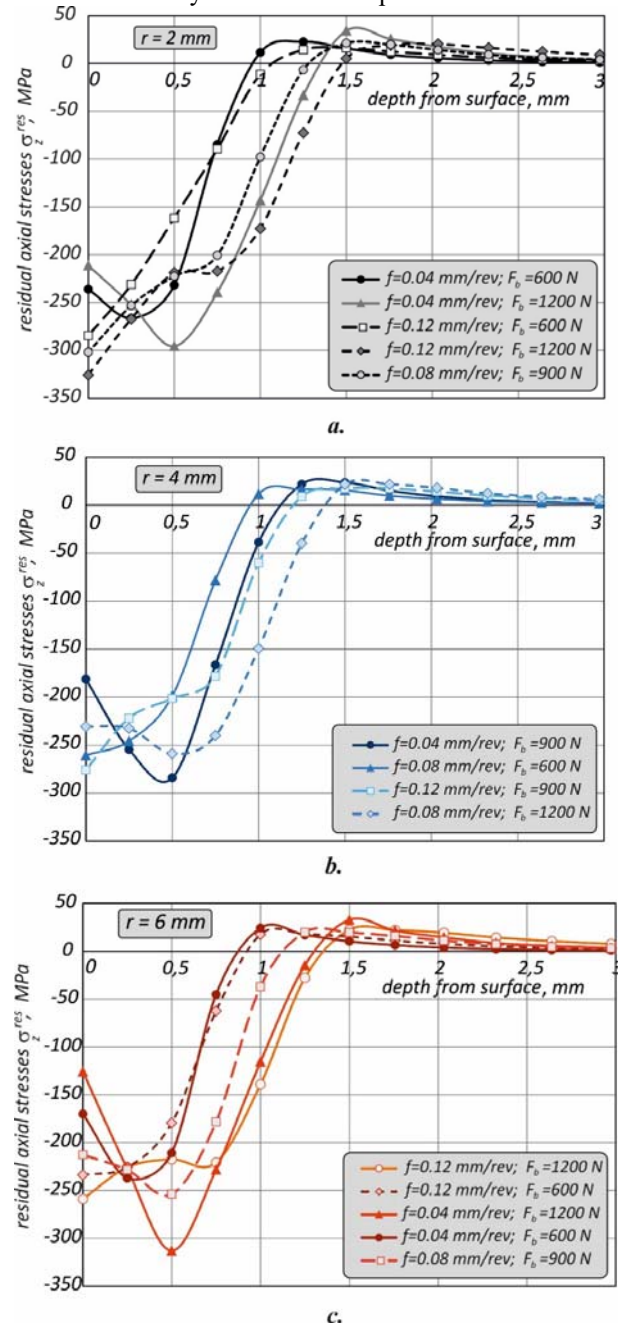


Fig. 4. Distribution of residual stresses  $\sigma_z^{res}$  in a depth

Parameters of the X-ray experiment were as follows: range  $134\text{--}144^\circ 2\theta$ ; step:  $0.4^\circ 2\theta$ ; tilt:  $\sin^2\psi = 0, 0.15, 0.3, 0.45, 0.6$  of both positive and negative values of angle  $\psi$ . Using the mentioned size of pinhole and parameters of experiment, the maximum length of irradiated area was 7

mm. The comparison for the residual axial stresses  $\sigma_z^{res}$  distribution obtained from the FE model and X-ray diffraction measurement is shown in Fig. 6. Fig. 6 shows good agreement between X-ray and FE results with respect to the residual axial stresses in a depth 0.6 mm from the surface layer. As is often the case with such kind of comparisons, FE results show raised absolute values of the residual stresses. Probably one of the reasons is in the essence of the FE method itself. Each deformable solid has a countless number of degrees of freedom. The restraint of these degrees is of equal worth to introduction of additional connections, which leads to an increase in the body stiffness in comparison with the actual one.



Fig. 5. A specially designed deep rolling device with a toroidal roller

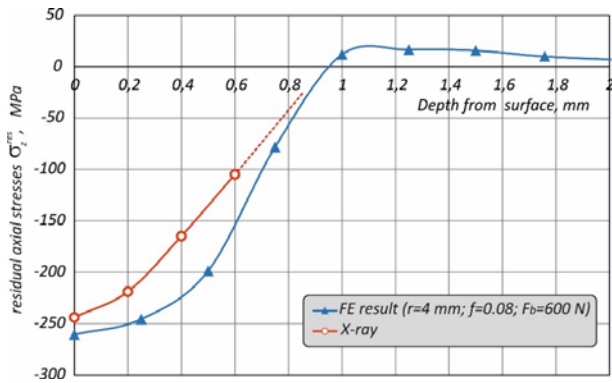


Fig. 6. Comparison for residual axial stresses distribution obtained from FE results and X-ray diffraction measurement

2.5. Analysis of Variance (ANOVA)

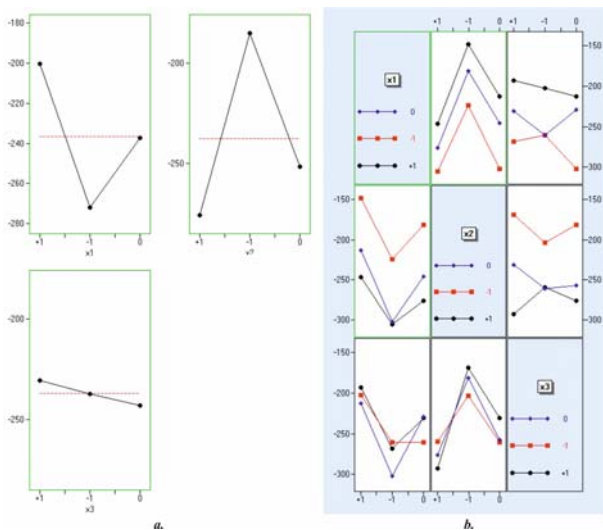


Fig. 7. Results obtained from ANOVA for  $\sigma_{z,sur}^{res}$   
a. main effects; b. interactions between factors

A dispersion analysis (ANOVA) was performed to assess the influence of factors on the two objective

functions using QStatLab [47]. Fig. 7 and Fig. 8 show the main effects and the interactions between the three factors.

Obviously, the feed rate  $f(x_2)$  is the factor with the greatest influence on the residual axial stress distribution on the surface (Fig.7a). The influence of the radius of curvature on the roller  $r$  is commensurate with that of the feed  $f$ , as the function of  $\sigma_{z,sur}^{res}$  depends in less degree on the burnishing force  $F_b$ . The interaction between the radius of curvature of the roller  $r$  and the feed  $f$  ( $x_1$  and  $x_2$ ) is the strongest (Fig. 7b).

The governing factors have a different impact on the residual axial stress distribution at a depth of 0.5 mm from the surface (Fig.8). The function of  $\bar{\sigma}_z^{res}$  depends to a large extent on the burnishing force  $F_b$  and at least on the feed rate  $f$ . Expected, the factors  $F_b$  and  $r$  have an opposite effect on the mean value of  $\sigma_z^{res}$ , which was determined for subsurface layers. The function of  $\bar{\sigma}_z^{res}$  is the highest in absolute value when the process is carried out with maximum burnishing force, minimum roller radius and mean value for feed rate ( $F_b = 1200 N$ ,  $r = 2 mm$ ,  $f = 0.08 mm/rev$ ). The interaction between the radius of curvature of the roll  $r$  and the burnishing force  $F_b$  is the strongest (Fig.8b).

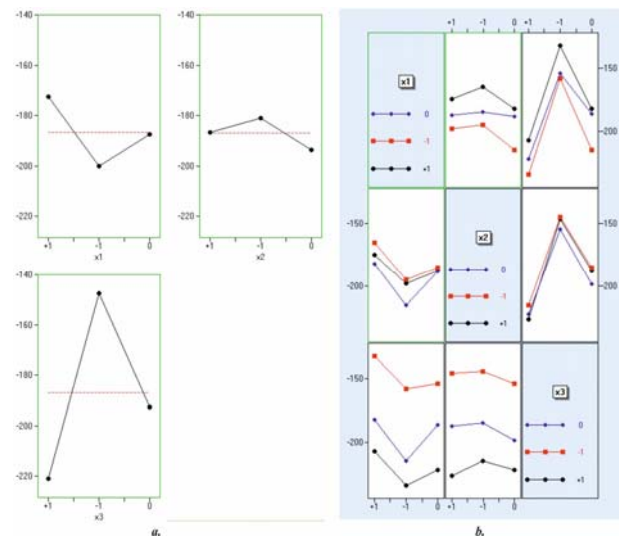


Fig. 8. Results obtained from ANOVA for  $\bar{\sigma}_z^{res}$   
a. main effects; b. interactions between factors

2.6. Regression analysis

Using QStatLab system [47] a regression analysis was performed on the basis of Table 2. The following regression models for the two objective functions in coded form were obtained:

$$F(\sigma_{z,sur}^{res}) = -250.463 + 44.61x_1 - 47.3x_2 + 15.05x_3 - 6.947x_1^2 + 21.793x_2^2 + 4.743x_3^2 - 4.204x_1x_2 - 16.924x_2x_3 + 4.426x_1x_3 + 14.696x_1^2x_3 - 11.006x_1x_2^2 + 2.309x_1^2x_2 \tag{4}$$

$$F(\bar{\sigma}_z^{res}) = -195.127 + 16.485x_1 - 33.98x_3 - 3.618x_1^2 + 8.812x_2^2 + 6.747x_3^2 + 2.054x_1x_2x_3 - 2.414x_2x_3 - 3.211x_2x_3^2 - 1.649x_1x_2 - 3.694x_1^2x_3 - 3.174x_1x_3^2 \tag{5}$$

In order to analyze the regression models (4) and (5), sections of their hyper-surfaces with different hyperplanes are shown, respectively, in Fig. 9 and Fig. 10. Graphs predict the change of the functions  $F(\sigma_{z,sur}^{res})$  and  $F(\bar{\sigma}_z^{res})$  when the third factor has an average value.

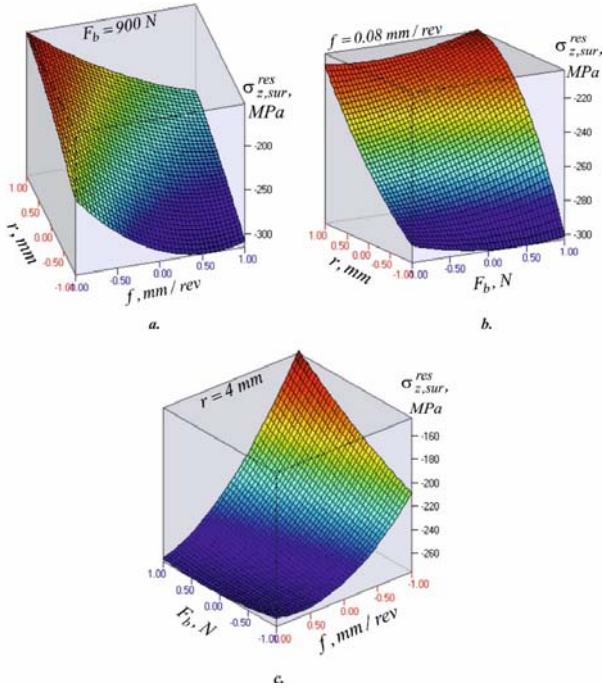


Fig. 9. Sections of the hyper-surface of the  $F(\sigma_{z,sur}^{res})$  model with different hyper-planes

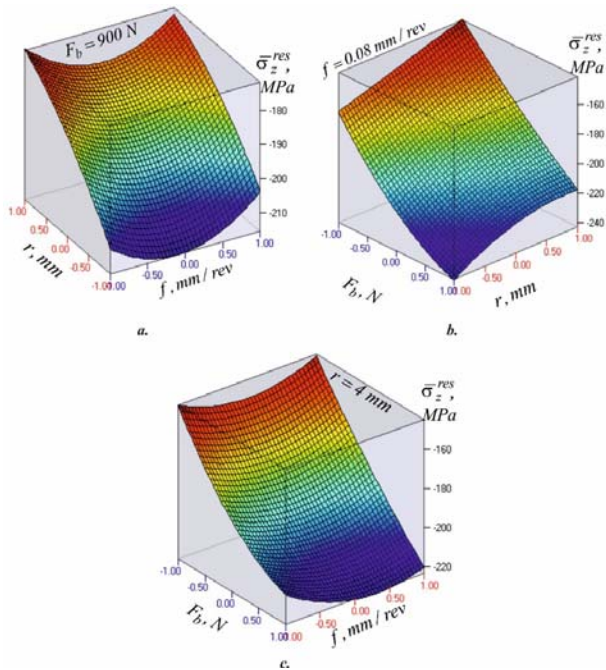


Fig. 10. Sections of the hyper-surface of the  $F(\bar{\sigma}_z^{res})$  model with different hyper-planes

### 3. OPTIMIZATION OF THE PROCESS IN TERMS OF RESIDUAL AXIAL STRESSES

In order to provide a maximum intensive and deep compressive zone with residual axial stresses  $\sigma_z^{res}$ , an

optimization of the deep rolling process with toroidal roller was carried out based on the obtained regression models (4) and (5). The optimization is directed to minimizing the two objective functions:

$$F(\sigma_{z,sur}^{res}) \rightarrow \min ; F(\bar{\sigma}_z^{res}) \rightarrow \min ; \tag{6}$$

The optimization was performed through the QStatLab system using a genetic algorithm. Taking into account the significance of the compressive residual axial stresses on the surface, the priority is given to the  $F(\sigma_{z,sur}^{res})$  function. The optimal solution that defines the values of the governing factors and their corresponding objective functions is shown in Table 4. The dependence between the factors in coded form  $x_i$  and natural coordinates  $\tilde{x}_i$  is:

$$x_i = (\tilde{x}_i - \tilde{x}_{0,i}) / \lambda_i, \tag{7}$$

where  $\lambda_i = (\tilde{x}_{max,i} - \tilde{x}_{min,i}) / 2$ ,  $\tilde{x}_{0,i}$ ,  $\tilde{x}_{max,i}$  and  $\tilde{x}_{min,i}$  are respectively the mean, upper and lower level of the  $i$ -th factor in natural coordinates.

Table 4 Optimization results

$r, mm$ ( $x_1$ )		$f, mm/rev$ ( $x_2$ )		$F_b, N$ ( $x_3$ )		$F(\sigma_{z,sur}^{res}), MPa$	$F(\bar{\sigma}_z^{res}), MPa$
Cod	Nat	Cod	Nat	Cod	Nat	-326,7267	-241,3709
-0,9999	2	0,8893	0,115	0,9999	1200		

### 4. CONCLUSIONS

Based on the developed 3D FE model of the deep rolling process with a toroidal profiled roller a planned numerical experiment was conducted to model the residual axial stresses in 2024-T3 high-strength aluminum alloy. In order to study the influence of the radius of curvature on the roller, the feed rate, and the burnishing force the following was conducted: dispersion analysis, regression analysis, and two-objective process optimization were performed. Based on the results obtained the following main conclusions can be made:

- In order to create maximum in absolute values residual surface axial stresses, it is advisable the process to be conducted with a minimum radius, maximum feed rate and maximum burnishing force:

$$r = 2 mm ; f = 0.12 mm/rev ; F_b = 1200 N ;$$

- For all studied roller radius, the combination of minimum feed rate ( $r = 2 mm$ ) and maximum burnishing force ( $F_b = 1200 N$ ) introduced maximum in absolute value stresses  $\sigma_z^{res}$  at a depth of  $0.5 mm$  from the surface;

- The optimal values of the process parameters are determined providing an intensive zone with compressive residual axial stresses on the surface and in depth of  $0.5 mm : r = 2 mm ; f = 0.115 mm/rev ; F_b = 1200 N$ .

### ACKNOWLEDGEMENT

The authors especially thank prof. Nikolay Ganev from the Technical university in Prague for his contribution in the X-ray diffraction measurement.

### REFERENCE

[1] M'Saoubi R., A review of surface integrity in machining and its impact on functional performance and life of machined

- products. *Int. J. Sustainable Manufacturing*, 1 (1-2)(2008) 203-236.
- [2] Maximov J.T., Duncheva G.V., Anchev A.P., Fatigue Life Increase of 2024-T3 Aluminium Alloy by Slide Burnishing. LAP Lambert Academic Publishing, Saarbrücken, 2017.
- [3] Maximov J.T., Anchev A.P., Dunchev V.P., N. Ganev, Duncheva G.V., Selimov K. F., Effect of slide burnishing basic parameters on fatigue performance of 2024-T3 high-strength aluminium alloy, *Fatigue Fract. Eng. Mat. Struct.* 40 (11) (2017) 1893-1904.
- [4] Maximov J.T., Anchev A. P., Duncheva G. V., Ganev N., Selimov K. F., Dunchev V. P., Impact of slide diamond burnishing additional parameters on fatigue behaviour of 2024-T3 Al alloy. *Fatigue Fract. Eng. Mat. Struct.* (2018) 363-373.
- [5] Maximov J.T., Anchev A. P., Duncheva G. V., Ganev N., Selimov K. F., Influence of the process parameters on the surface roughness, micro-hardness, and residual stresses in slide burnishing of high-strength aluminum alloys, *J. Braz. Soc. Mech. Sci. Eng.* 39(8) (2017) 3067-3078.
- [6] Maximov J.T., Duncheva G. V., Anchev A. P., Ganev N., Amudjev I. M., Dunchev V. P., Effect of slide burnishing method on the surface integrity of AISI 316Ti chromium-nickel steel. *Journal of the Brazilian Society of Mechanical Sciences and Engineering* (2018) 40 194 DOI:10.1007/s40430-018-1135-3.
- [7] Maximov J.T., Duncheva G.V., Anchev A.P., Amudjev I.M., Kuzmanov V.T. Enhancement of fatigue life of rail-end-bolt holes by slide diamond burnishing. *Engineering Solid Mechanics* 2 (4) (2014) 247-264.
- [8] Ecoroll Catalogue "Tools & Solutions for Metal Surface Improvement". Ecoroll Corporation Tool Technology, USA, 2006.
- [9] Malleswara Rao J.N., Chenna Kesava Reddy A., Rama Rao P. V., Study of Roller Burnishing process on Aluminum Work Pieces Using Design of Experiments. *International Journal of Mechanical Engineering and Technology*, 2 (1) (2011) 777-785.
- [10] Drechsler A., Kiese J., Wagner L., Effects of Shot Peening and Roller Burnishing on Fatigue Performance of various Titanium Alloys. The 7 th International Conference of Shot Peening, Poland (1999) 145-152.
- [11] Othman O.A., Basha M., Wagner L., Optimizing the Process Parameters and Investigating the Influence of Shot Peening and Roller Burnishing on Surface Layer Properties and Fatigue Performance of Al 6061 T4. *Sohag J. Sci.* 1 (1) (2016) 65-72.
- [12] Kiran A. Patel, Pragnesh K. Brahmhatt, Surface Roughness Prediction for Roller Burnishing of Al Alloy 6061 Using Response Surface Method. *International Journal of Scientific & Engineering Research* 6 (3) (2015) 636-640.
- [13] Al-Qawabena U.F., Al-Qawabah S.M., Effect of roller burnishing on pure aluminum alloyed by copper. *Industrial Lubrication and Tribology* 65 (2)(2013) 71-77.
- [14] Lindemann J., Glavatskikh M., Leyensl C., Oehring M., Appel F., Influence of Mechanical Surface Treatments on the High Cycle Fatigue Performance of Gamma Titanium Aluminides. In: *Ti-2007 Science and Technology*, edited by M. Ninomi, S. Akiyama, M. Ikeda, M. Hagiwara, K. Maruyama. The Japan Institute of Metals (2007) 1703-1706.
- [15] Abrão A.M., Denkena B., Köhler J., Breidenstein B., Mörke T., The influence of deep rolling on the surface integrity of AISI 1060 high carbon steel. *Procedia CIRP* 13 (2014) 31 – 36
- [16] Chomienne V., Valiorgue F., Rech J., Verdu C., Influence of ball burnishing on residual stress profile of a 15-5PH stainless steel. *CIRP Journal of Manufacturing Science and Technology* 13 (2016) 90–96.
- [17] Gomez-Gras G., Travieso-Rodriguez J.A., Jerez-Mesa R., Experimental characterization of the influence of lateral pass width on results of a ball burnishing operation. *Procedia Engineering* 132 (2015) 686 – 692.
- [18] Mombeini D., Atrian A., Investigation of Deep Cold Rolling Effects on the Bending Fatigue of Brass C38500. *Latin American Journal of Solids and Structures*, 15(4) (2018)1/19-19/19.
- [19] Majzoobi G. H., Jouneghani F. Z., Khademi E., Experimental and numerical studies on the effect of deep rolling on bending fretting fatigue resistance of Al7075. *The International Journal of Advanced Manufacturing Technology* 82 (9-12) (2016) 2137-2148.
- [20] Bouzid Sai W., Lebrun J.L., Influence of Finishing by Burnishing on Surface Characteristics, *Journal of Materials Engineering and Performance* 12 (1) (2003)37-40.
- [21] Wagner L., Mhaede M., Wollmann M., Altenberger I., Sano Y., Surface layer properties and fatigue behavior in Al 7075-T73 and Ti-6Al-4V. Comparing results after laser peening; shot peening and ball-burnishing. *International Journal of Structural Integrity* 2 (2) (2011) 185-199.
- [22] Shiou F.J., Hsu C.C., Surface finishing of hardened and tempered stainless tool steel using sequential ball grinding, ball burnishing and ball polishing processes on a machining centre. *Journal of Materials Processing Technology* 205 (2008) 249–258.
- [23] Firas M. F. Al Quran, The Effect of Roller Burnishing on Surface Hardness and Roughness of Aluminum Alloy. *International Journal of Mechanics and Applications* 5(2) 2015 37-40.
- [24] Dwivedi S. P., Sharma S., Mishra R. K., Effects of roller burnishing process parameters on surface roughness of A356/5%SiC composite using response surface methodology. *Adv. Manuf.* 2 (2014)303–317.
- [25] Nestler A., Schubert A., Roller Burnishing of Particle Reinforced Aluminium Matrix Composites. *Metals* 8 (2) (2018) 95; doi:10.3390/met8020095.
- [26] Malleswara Rao J. N., Chenna Kesava Reddy A., Rama Rao P. V., The effect of roller burnishing on surface hardness and surface roughness on mild steel specimens. *International Journal of Applied Engineering Research* 1 (4)(2011) 777-785.
- [27] Zaroog O. S., Ali A., Sahari B.B., Zahari R., Modeling of residual stress relaxation of fatigue in 2024-T351 aluminium alloy. *International Journal of Fatigue* 33 (2011) 279-285.
- [28] Maximow J.T., Duncheva G. V., Mitev I.N., Modelling of residual stress relaxation around cold expanded holes in carbon steel. *Journal of Constructional Steel Research* 65 (2009) 909-917.
- [29] Zhuang W., Halford G., Investigation of residual stress relaxation under cyclic load, *International Journal of Fatigue* 23 (2001) 31-37.
- [30] Kwofie S., Description and simulation of cyclic strain-stress response during residual stress relaxation under cyclic load. *Procedia Engineering* 10 (2011) 293-298.
- [31] Roettger K., Walzen hargedrehter oberflaechen, PhD Thesis, WZL, RWTH Aachen, University, Aachen, Germany, 2002.
- [32] Sai WB, Sai K, Finite element modeling of burnishing of AISI 1042 steel. *Int J Adv Manuf Technol* 25 (5-6) (2005)460–465.
- [33] Bougharriou A., SaiWB, Sai K., Prediction of surface characteristics obtained by burnishing. *Int J Adv Manuf Technol* 51 (1-4) (2010)205–215.
- [34] Yen Y. C., Sartkulvanich P., Altan T., Finite Element Modeling of Roller Burnishing Process, *CIRP Annals – Manuf. Technol.* 54 (1) (2005) 237-240.
- [35] Sartkulvanich P., Altan T., Jasso F., Rodriguez C., Finite element modeling of hard roller burnishing: an analysis on the effects of process parameters upon surface finish and residual stresses. *J. Manuf. Sci. Eng.* 129 (4) (2007) 705-716.

- [36] Balland P., Tabourot L., Degre F., Moreau V., An investigation of the mechanics of roller burnishing through finite elementsimulation and experiments. *International Journal of Machine Tools & Manufacture* 65 (2013) 29–36.
- [37] Trauth D., Klocke F., Mattfeld P., Klink A., Time-Efficient Prediction of the Surface Layer State after DeepRolling using Similarity Mechanics Approach. *Procedia CIRP* 9 (2013) 29 – 34.
- [38] Sayahi M, Sghaier S, Belhadjsalah H, Finite element analysis of ball burnishing process: comparisons between numerical results and experiments. *Int J Adv Manuf Technol* 67 (5-8) (2013)1665–1673.
- [39] Mohammadi F., Sedaghati R., Bonakdar A., Finite element analysis and design optimization of low plasticity burnishing process. *Int J Adv Manuf Technol* 70 (5-8) (2014)1337–1354.
- [40] Zhuang W., Wicks B., Multi-pass Low Plasticity Burnishing Induced Residual Stresses: Three-dimensional Elastic-plastic Finite Element Modelling. *Journal of Mechanical Engineering Science, ImechE Part C* 218 (2004) 663-668.
- [41] Saldana-Robles A., Aguilera-Gomez E., Plascencia-Mora H., Ledesma-Orozco E.R. RevelesArredondo F.J., Saldana-Robles N., FEM Burnishing Simulations Including Roughness, *Mechanik* 2 (2015) 79-91.
- [42] Stalin John M.R., Welsoon A.W., Prasad A.B., Avinav Abraham, B.K, Vinayagam, An Investigation of ball burnishing process on CNC lathe using finite element analisys. *Simulation Modelling Practice and Theory* 62 (2016) 88-101.
- [43] Di He, Bin Wang, Jiayang Zhang, Shaofeng Liao, Wen Jun Deng, Investigation of interference effects on the burnishing process. *Int J Adv Manuf Technol* 95 (1-4) (2018)1–10.
- [44] Duncheva G.V., Atanasov T.P., Anchev A.P., Finite Element Modeling of the Superficial Layer Strained State of 2024-T3 Aluminum Alloy Subjected to Roller Burnishing. *National Conference of Machine Building and Mechanical Engineering, Days of Mechanics in Varna, 8-10 September (2018) (in Bulgarian).*
- [45] Anchev A.P., Atanasov T.P., Duncheva G.V., Surface Layer Constitutive Model of 2024-T3 Anuminum Alloy Subjected to Surface Plastic Deformation. *National Conference of Machine Building and Mechanical Engineering, Days of Mechanics in Varna, 8-10 September (2018) (in Bulgarian).*
- [46] Duncheva G.V., Synthesis and Optimization of Methods for Increasing the Fatigue Life of Metal Structures with Holes. *DSc Dissertation Theses (2017) (in Bulgarian).*
- [47] Vuchkov I. N. and Vuchkov I. I. *QStatLab Professional, v. 5.5 – statistical quality control software. User’s Manual, Sofia, 2009*